Available online at www.sciencedirect.com
SCIENCE DIRECT®
Earth and Planetary Science Letters 242 (2006) 302–319
EPSL
www.elsevier.com/locate/epsl

# Hydrogen loss from olivines in mantle xenoliths from Simcoe (USA) and Mexico: Mafic alkalic magma ascent rates and water budget of the sub-continental lithosphere

Anne H. Peslier [a,*], James F. Luhr [b]

[a] Texas Center for Superconductivity at the University of Houston (TcS-UH), HSC Building 202, Houston, TX 77204, USA
[b] Department of Mineral Sciences, Smithsonian Institution, P.O. Box 37012, NHB-119, Washington, DC 20013, USA

Received 10 September 2005; received in revised form 15 December 2005; accepted 15 December 2005
Available online 26 January 2006
Editor: R.W. Carlson

**Abstract**

Olivines in spinel-peridotite mantle xenoliths from Simcoe (Washington State, USA) and Mexico were analyzed by Fourier-transform infrared spectrometry (FTIR) to determine their water contents. The main OH absorbance peaks of most samples are located between 3600 and 3450 $cm^{-1}$ (Group I), with a few samples having minor peaks between 3450 and 3100 $cm^{-1}$ (Group II). Olivines from one Mexican sample have larger peaks in Group II than in Group I. Most of these OH peaks are predicted by experimental data from the literature in the appropriate range of silica activities and iron contents. A few high-forsterite olivines, however, have mainly Group I peaks which at these low iron contents is characteristic of low-silica activity. Because these olivines coexist with orthopyroxene in the peridotite, buffering silica activity at relatively high values, their FTIR spectra may reflect disturbance of their hydrogen by melts or fluids, most probably associated with the host magma. In eight out of nine samples for which measurement at the olivine edges was possible, water contents are higher in the grain centers than at their edges, with cross-sections showing typical diffusion profiles. Moreover, water concentrations in some samples increase with olivine size. Loss of hydrogen from the olivine during xenolith transport to the surface is likely responsible for these variations. These water-concentration gradients allowed calculation of the duration of hydrogen loss, which ranges from 18 to 65 h, corresponding to host mafic-alkalic magma ascent rates of 0.2–0.5 m $s^{-1}$. The highest measured water contents in olivines from individual xenoliths range from 0 to 6.8 ppm and increase with those of clino- and orthopyroxenes. Differences in hydrogen partition coefficients between olivine and pyroxenes from our data and from experiments suggest that the analyzed olivines lost at least 40% of their water during ascent from the mantle. Olivine water contents do not correlate with partial melting indices, but samples with high olivine water contents generally have low clinopyroxene La/Yb ratios and low spinel $Fe^{3+}/\Sigma Fe$ ratios and resultant oxygen fugacities, and vice-versa. Metasomatism by fluids or melts and the ambient oxygen fugacity of the mantle may have played roles in the original incorporation of hydrogen into these olivines, but such primary signals have probably been obscured by later hydrogen loss. The systematically lower water contents of olivines in Mexican and Simcoe xenoliths relative to those from cratonic xenoliths may mainly reflect lower host-magma ascent velocities for mafic alkalic magmas compared to kimberlites. Calculated whole-rock water contents for the studied spinel-peridotite xenoliths range from 2.5 to 154 ppm. If 150 ppm were

* Corresponding author.
*E-mail addresses:* apeslier@mail.uh.edu (A.H. Peslier), luhr@volcano.si.edu (J.F. Luhr).

0012-821X/$ - see front matter 
doi:10.1016/j.epsl.2005.12.019

representative of the water content in the entire upper mantle (to 410 km), the amount of water stored there can be speculated to be only about 0.06 times the equivalent mass of Earth's oceans.


*Keywords:* water; olivine; xenolith; hydrogen loss; host-magma ascent rate; continental upper-mantle

## 1. Introduction

Olivine is the main mineral phase of Earth's mantle to a depth of 410 km, typically making up 55–95% by weight of peridotite, the dominant rock-type in the upper-mantle. Although nominally anhydrous, olivine can accommodate small amounts of "water", characteristically <5–100 ppm in natural samples [1,2], as hydrogen protons inserted in mineral defects and vacancies. These apparently trivial water contents actually have a disproportionate influence on many physical and chemical properties of olivine, and therefore on that of the entire upper-mantle. In particular, the presence of bound hydrogen in the structure of upper-mantle minerals can lower their viscosity [3–6], enhance their radiative transfer [7], attenuate seismic waves [8], increase their electrical conductivity [9,10], and lower melting temperatures and affect the speciation of fluid or melt [11,12]. Because key geodynamic processes find their origin in the upper-mantle, from plate tectonics to magma generation, it is crucial to determine the nature and abundance of water in its dominant phase. This paper presents Fourier-transform infrared (FTIR) spectrometry data on water in olivine from spinel-peridotite xenoliths. They represent typical sub-continental lithospheric mantle that underlies Phanerozoic terranes outside cratons, and that possibly underwent various degrees of interaction with subduction-related melts or fluids. Three main questions are addressed: (1) How well do the water contents measured in these olivines reflect the primary mantle values prior to xenolith transport to the surface? (2) What additional processes might have affected the range of water contents observed? and (3) What is the water budget of the sub-continental upper-mantle?

The extensive literature on FTIR spectra of olivine from various types of rocks emphasizes the complicated nature of the OH bands, debates as to where hydrogen is located in the olivine structure, and describes frequent micro-inclusions of various water-rich minerals [13–21]. The solubility of hydrogen in olivine has been estimated experimentally to range from >46 to >5300 ppm $H_2O$ [15,22–27], and diffusion experiments show that hydrogen can move very quickly through olivine at magmatic temperatures [3,28]. For peridotite xenoliths, natural olivines analyzed for water content have come from isolated samples from various locations around the world [1,20,25,29]. Water concentrations of all the minerals of the peridotite are reported only for 7 mantle xenolith samples [1,2]. The present paper provides water contents in olivines from spinel peridotites for which the pyroxene water contents have been already published [30], including data for several samples from each mantle-xenolith suite. This data set is the most extensive so far on typical off-craton sub-continental lithospheric mantle.

## 2. Geological setting

The analyzed olivines are from spinel-peridotite xenoliths hosted by various mafic alkalic volcanic rocks (alkali basalts, basanites, and olivine nephelinites) [30]. The peridotites are typical Cr-diopside bearing Type-I peridotites [31], and are interpreted to result from various degrees of partial melting in the mantle. The host magmas erupted during Plio-Pleistocene time through Phanerozoic lithosphere. These peridotites are thus representative of off-craton sub-continental lithospheric mantle.

The shield volcano of Simcoe is located 200 km north of the northern edge of the US Basin and Range province, and 65 km east of the Cascade Range. Subduction has been occurring for about 50 Ma in this region [32]. Multiple evidence (petrology, trace elements, oxygen fugacity, Sr–Nd–Pb–Os isotopes) shows that the Simcoe peridotites, all harzburgites, have seen the influence of melts or fluids from the slab (Farallon plate) by multi-stage processes spanning 10 Ma, and thus represent mantle wedge material [33–36].

The Mexican xenoliths were sampled at 5 locations spanning a NW–SE 1700 km transect across the Basin and Range province of Mexico: San Quintín, Mesa Cacaxta, Durango, Ventura-Espiritu Santo, and Santo Domingo. The host magmas erupted through an assemblage of different tectonic terranes accreted to the North American craton from the late Paleozoic to the early Cenozoic [37]. Subduction at the western edge of this region has occurred during most of Mesozoic and Cenozoic time. The mantle represented by these peridotites has been influenced to various degrees by subduction-related melts or fluids [37]. The peridotites

classically range from fertile lherzolites to depleted harzburgites. One Ventura-Espiritu Santo sample, SLP400, is unique in containing glass-rich, phlogopite bearing veinlets and having relatively Fe-rich olivines (forsterite content $Fo_{81.5}$) and pyroxenes. At Santo-Domingo, the analyzed peridotite xenoliths were accompanied by abundant mantle-derived kaersutite megacrysts and kaersutite-pyroxenite xenoliths, some as composite xenoliths with peridotite.

## 3. Analytical techniques

### 3.1. Sample preparation and analysis by FTIR

The olivines analyzed in this study were disaggregated from central portions of the peridotite xenoliths. Epoxy wafers of 20–30 grains per sample of clear olivines were polished on two parallel sides. Only the grains oriented Bxo, Bxa or optic normal, determined using interference figures on a petrographic microscope, were analyzed by FTIR. In two of our analyzed samples (BCN201, SIN3), all the olivine grains were riddled with very tiny fluid inclusions so that FTIR analysis avoiding them was not possible. Olivine thicknesses, measured using a Mitutoyo digital micrometer (ID-C112CEB), ranged from 0.2 to 1.5 mm.

Olivines were analyzed with a Nicolet NEXUS 670FT FTIR coupled with a Continuum Microscope at NASA-Johnson Space Center's Astromaterials Research and Exploration Science Division. All measurements were made with a Zn–Se wire grid polarizer and a nitrogen-cooled Hg–Cd–Te (MCT) detector with a range of 4000–680 $cm^{-1}$. To avoid surface contamination by room-air humidity, samples were kept before analysis at least 1 h in a dessicator and, when located on the microscope stage, were continuously flushed in pure nitrogen gas. The number of scans was typically 128, but water-poor olivines were run with up to 500 scans. The resolution was always set at 4 $cm^{-1}$. Most analyses were made with an apertured area of $150 \times 150$ μm, but some were smaller (down to $50 \times 50$ μm). At least 3 grains per sample were analyzed, and for each grain, at least 3 areas at the grain center were analyzed. When analysis was possible near the grain edge, profiles across the entire grain were made. Proper quantification of water content in an anisotropic mineral can only be achieved by analyzing it in 3 perpendicular directions [38], in our case with the infrared polarizer (*E*) parallel to the optical indicatrix indices alpha or section [010], beta or [001], and gamma or [100].

Spectra were processed using the Omnic software that controls the Nicolet FTIR. All spectra had sinusoidal backgrounds that varied in wavelength for each sample, each grain, and each direction. These are likely interference patterns of the infrared light hitting microscopic imperfections within the olivine. Simple background subtraction of dehydrated olivine was therefore not possible. In order to obtain a flat baseline, the background was manually drawn beneath the O–H stretching vibration peaks (Fig 1) using the spline correction of the Omnic software. Another method would be to try to fit a mathematical function to the sinusoidal background, but manual fitting, although subjective, appears to give comparable results [25]. The area tool of the Omnic software was then used to measure the area beneath the OH peaks, typically between 3700 and 3100 $cm^{-1}$.

The Beer-Lambert law allows calculation of water contents from the FTIR spectra with water concentration = area beneath OH peaks/thickness × absorption coefficient. The most appropriate absorption coefficient for this study is that determined by Bell et al. [25] for forsteritic olivine. More exactly, their equation

$$H_2O \text{ (ppm by weight)} = 0.188 \times \text{Abs} \quad (1)$$

was used with Abs being the sum of the area beneath OH peaks in all 3 directions ($\alpha$, $\beta$, $\gamma$) on spectra normalized to 1 cm. Special discussion is necessary for Mexican peridotites SLP114 and SLP400, both from Ventura-Espiritu Santo, whose olivines do not have their main absorption intensities in the 3700–3450 $cm^{-1}$ region like all other samples. Those of harzburgite SLP114 are in the 3450–3100 $cm^{-1}$ region. Phlogopite-lherzolite SLP400 has Fe-rich olivines ($Fo_{81.5}$) with a broad absorption band centered around 3250 $cm^{-1}$ in the $\gamma$ direction, whose contribution in absorbance area is greater than those of the peaks located between 3700 and 3450 $cm^{-1}$. The Bell et al. [25] calibration is only valid for olivines with their largest absorptions in the 3700–3450 $cm^{-1}$ region, and thus cannot be applied to SLP114 and SLP400. Although not experimentally determined, it is anticipated that for such olivines, the absorption coefficient might be 2.3–2.5 times higher than that used in Eq. (1) [25]. The calculation of water content in Eq. (1) for these two samples was accordingly made with a constant of 0.188/2.4 so as to not overestimate their water contents.

### 3.2. Uncertainties

Uncertainty on the orientation of minerals on a polarizing microscope is estimated to be ±5%. Repeated measurements of the thicknesses of olivine grains yield

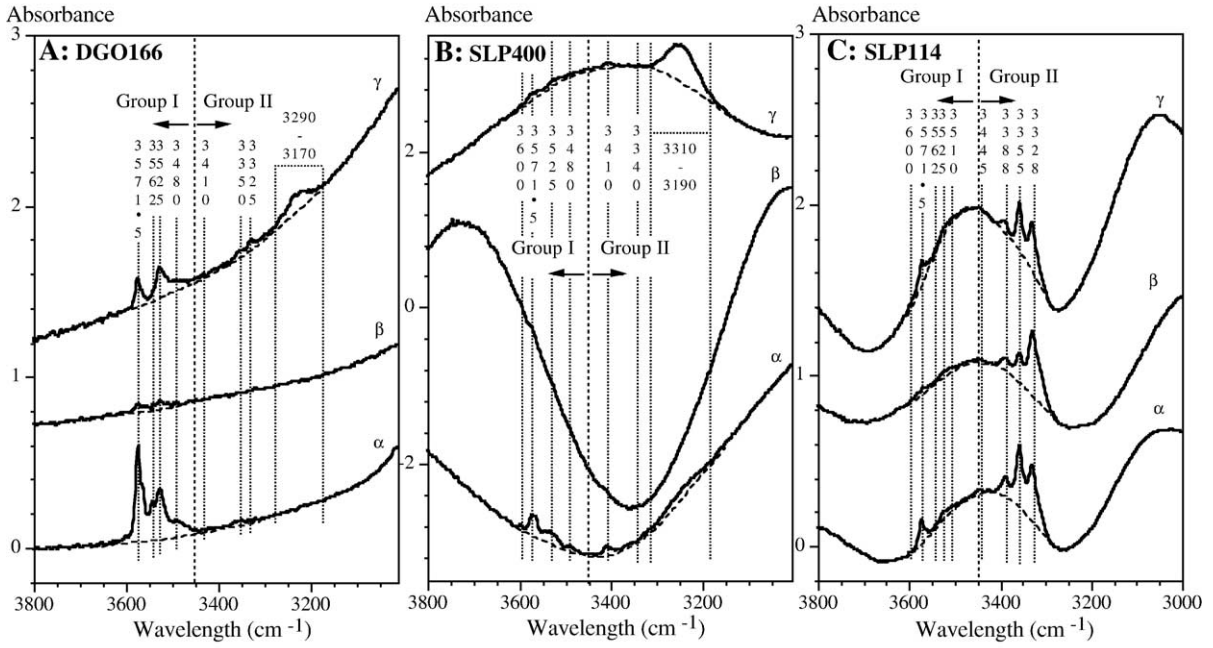


Fig. 1. Polarized transmission FTIR spectra normalized to 1 cm for olivines from Mexican xenoliths DGO166 (A), SLP400 (B), and SLP114 (C) in the OH-stretching vibration region. $\alpha$, $\beta$, and $\gamma$ denote the orientation of the polarizer (see text). Group I and Group II are defined as the olivine spectral regions 3700–3450 $cm^{-1}$ and 3450–3100 $cm^{-1}$, respectively [22]. DGO166 has a spectrum representative of all other analyzed olivines except for SLP400 and SLP114, with main OH absorptions in Group I. Most of these samples, however, do not have any detectable peaks in Group II. SLP400 has Fe-rich olivines ($Fo_{81.5}$) and has a large absorption band centered around 3240 $cm^{-1}$ in Group II in the $\gamma$ direction. SLP114 is unique in having its main OH-absorption peaks in Group II. Wavy sinusoidal backgrounds, most obvious here for SLP400 and SLP114, are likely due to scattering and interferences of the infrared light by micro defects possibly arranged in planes in the olivines. Dashed lines under OH absorbance peaks show where background was taken to calculate area beneath the peaks to obtain water content of the olivines.

an uncertainty of about ±3 μm. The 0.188 factor in the equation above has an uncertainty of ±0.012 [25]. Accuracy should therefore be good as the absorption coefficient was determined specifically for olivines of composition very similar to the ones analyzed here. The largest uncertainties, however, comes from the determination of spectra backgrounds. Because the correction was done manually, it is difficult to give a precise number to the associated uncertainty. Repetition of the manual background correction on the Omnic software 2–4 times for a couple of samples, one in the higher water-content range, and one in the lower-water content range, yielded uncertainties of ±0.2 $cm^{-2}$. For peaks barely above background, this is equivalent to >30% uncertainty, but for well-defined peaks the uncertainty is less than ±7%, which would account for the precision. Another uncertainty enters when the OH peaks are located on a sinusoidal background, because determining the position of the background beneath OH peaks in a “trough” or on a “hump” is more ambiguous than for straight background segments. Accordingly, uncertainties were attributed case by case depending on the peculiarities of each spectrum. Finally, when OH peaks could not be distinguished from background noise in all three directions, a value of 0 ppm was assigned to that sample. The detection limit is thus estimated to be about 0.2 ppm $H_2O$ by weight.

## 4. Results

### 4.1. Olivine FTIR spectra

Infrared absorption peaks due to the stretching vibration of the O–H bond are located between 3700 and 3100 $cm^{-1}$ (Fig. 1). All analyzed samples but one have their largest OH peaks in the 3700–3450 $cm^{-1}$ region (Group I [22]). Two of these (DGO166 and Fe-rich SLP400) have also minor peaks between 3450 and 3100 $cm^{-1}$ (Group II [22]). One sample, SLP114, has OH peaks with the largest absorbance intensities in Group II and minor peaks in Group I. Finally, OH peaks could not be distinguished from background for 2 samples (Sim3 and BCN203). Group I peaks in all three directions are located at 3600±4 (not always present), 3571.5±4 (always the highest peak), 3541±4, 3562±4, 3525±4, and 3480±4 $cm^{-1}$. Group II peaks, when

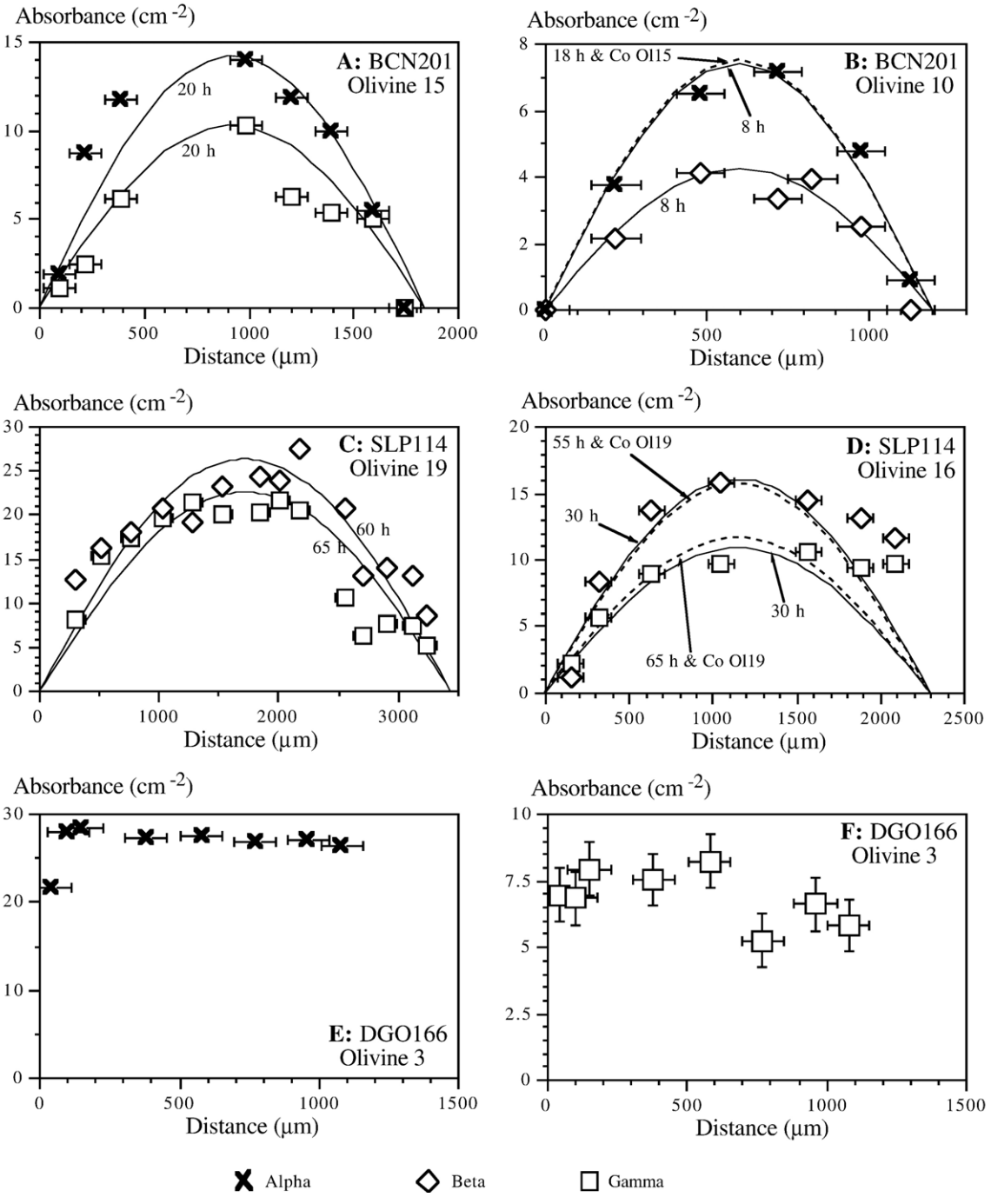


Fig. 2. Polarized infrared absorption intensities measured as area beneath the OH peaks across olivine grains from edge to edge. Analyses were made with an aperture of 150 μm (the "x error bar"), with the uncertainty on the absorbance for these olivines being 0.2 $cm^{-2}$ (about the size of the symbols except for DGO166 Olivine 3 gamma, panel F). The absorption is highest at the center of the olivines of BCN201 and lowest to absent at their edges. These typical diffusion profiles are interpreted to illustrate the loss of hydrogen undergone by the olivines during transport of the xenolith from the upper mantle to the surface by its host mafic alkalic magma. Crystals that do not show symmetrical patterns of rimward hydrogen loss (DGO166 Olivine 3, panels E and F, and one side of SLP114 Olivine 16, panel D) may not be true intact grain boundaries, but instead broken crystal edges generated when the xenoliths were disaggregated during sample preparation. In order to estimate the time of hydrogen loss, the profiles are modeled using Eq. (3) solved for the three terms of the series, a coefficient of hydrogen diffusion of $2.75\times10^{-12}$ m $s^{-1}$, and a $C_0$ of 40% more than that measured in the center of the olivine (see text for details). For BCN201 Olivine 10 alpha (B), and for SLP114 Olivine 16 beta and gamma (D) the model was run two ways; one using the $C_0$ measured at the center of the olivine (8 h and 30 h, respectively, solid lines) and one using the $C_0$ measured at the center of a larger olivine from the same xenolith (18 h and 55–65 h, respectively, dashed lines).

present, are located at 3410±4, 3345±5, 3340±4 or 3325±4 $cm^{-1}$ depending on the sample, and a broad band in the $\gamma$ direction between 3300 and 3190 $cm^{-1}$ (Fig. 1A and B). SLP114 has its main peaks in Group II at 3388±4, 3355±4 and 3328±4 $cm^{-1}$, and minor peaks in Group I at 3571.5±4, 3562±4, and 3525±4 $cm^{-1}$ (Fig. 1C). Relative heights vary from one direction to another. Relative intensities of the total integrated absorbances in the 3 directions are $\alpha>\gamma>\beta$ except for SLP114 where $\beta>\alpha>\gamma$, both these schemes being different from what has been observed in olivines before [14,40]. When water content is low, only the peak at 3571.5 $cm^{-1}$ is detectable.

### 4.2. Intra- and inter-olivine variations of water content

In most samples, absorption intensities of OH peaks are systematically lower or indistinguishable from background at the edges of olivine grains in all three directions (Appendix A). Cross sections of these olivines reveal bell-shaped profiles with the highest intensities in the grain centers (Fig. 2). Moreover, larger olivine grains have more hydrogen in their centers than do smaller grains for half of the samples, i.e. absorption intensities correlate with grain size (Fig. 3).

Stating the olivine water contents for each sample is thus complicated by these variations with position in the grain and grain size. In the following discussion, we emphasize the maximum determined water content for each sample, using the largest absorption intensities measured in each direction, which corresponds to the centers of 2 of the largest grains analyzed.

### 4.3. Water content variations

Maximum olivine water contents vary from 0 to 6.8 ppm (Table 1) and correlate with those of associated orthopyroxene and clinopyroxene [30] (Fig. 4). No correlation is observed between olivine water concentration and any compositional parameter in the olivine, including the forsterite content (Fig. 5), or in the peridotite, such as weight % $Al_2O_3$ in the bulk-rock. Although no clear correlation can be seen with clinopyroxene La/Yb ratio (Fig. 6) or spinel $Fe^{3+}/\Sigma Fe$ ratio (and calculated oxygen fugacity expressed as $\Delta$FMQ; Fig. 7), two groups of samples seem to define end-members. Simcoe ones have amongst the lowest olivine water contents and have high clinopyroxene La/Yb ratios and oxygen fugacities. Mexican samples from Santo Domingo have some of the highest olivine water contents coupled with low clinopyroxene La/Yb ratios and calculated oxygen fugacities.

## 5. Discussion

### 5.1. Group I versus Group II OH absorption bands

#### 5.1.1. Structurally bound hydrogen versus hydrogen-bearing inclusions

All olivine spectra except those for sample SLP114 are similar to previously published spectra for olivines from mantle samples [1,14,25,40,41]. No peaks >3600 $cm^{-1}$ are observed, meaning that no serpentine, talc, or dense hydrous magnesium silicate inclusions are present in these olivines [14,16,19]. Humite-group minerals would generate peaks that overlap with those of structural hydrogen in olivine and therefore it can only be assumed that these inclusions are not present [14]. All OH peaks are thus attributed to structurally bound protons in the olivine. Finally, it appears that the OH peaks obtained on olivines riddled with unavoidable fluid inclusions (BCN201, SIN3) are not due to water in the fluid inclusions (no identical molecular-water band centered at 3420 $cm^{-1}$ in all polarizer orientations) but are entirely due to hydrogen in the olivine structure (OH stretching bands vary with polarizer orientation). This is not surprising because most fluid inclusions from peridotites are dominantly filled with $CO_2$ [42].

#### 5.1.2. Generalities on Group I and Group II bands

Group I bands (3700–3450 $cm^{-1}$) and Group II bands (3450–3100 $cm^{-1}$) [15] are probably caused by the presence of hydrogen in 2 different point defects in the olivine structure, but the exact locations of these is still debated [13,15,28,43]. Typical spectra from natural olivines have their main absorption bands in Group I, and generally none in Group II [1,14,40]. Spectra with main absorption bands in Group II have been produced experimentally by annealing high-Mg olivines ($Fo_{\geq 90}$) in a high-silica activity environment [18,39] or at very high pressures (>13 GPa, [24]), or by using more Fe-rich olivines ($Fo_{\leq 88}$, [26]). High absorption in Group II also seems characteristic of natural olivines from silica-saturated volcanic rocks such as boninites [21]. In other words, a Fo-rich olivine in equilibrium with orthopyroxene should have a spectrum with the main peaks in Group II. Based on available experimental data, it is not possible to identify a precise forsterite content at which Group I bands start to dominate over Group II bands between $Fo_{88}$ (Group I dominates [24,26]) and $Fo_{90}$ (Group II dominates [18,26]). The olivines analyzed here coexist with Mg-rich orthopyroxene, clinopyroxene, and spinel [37,44].

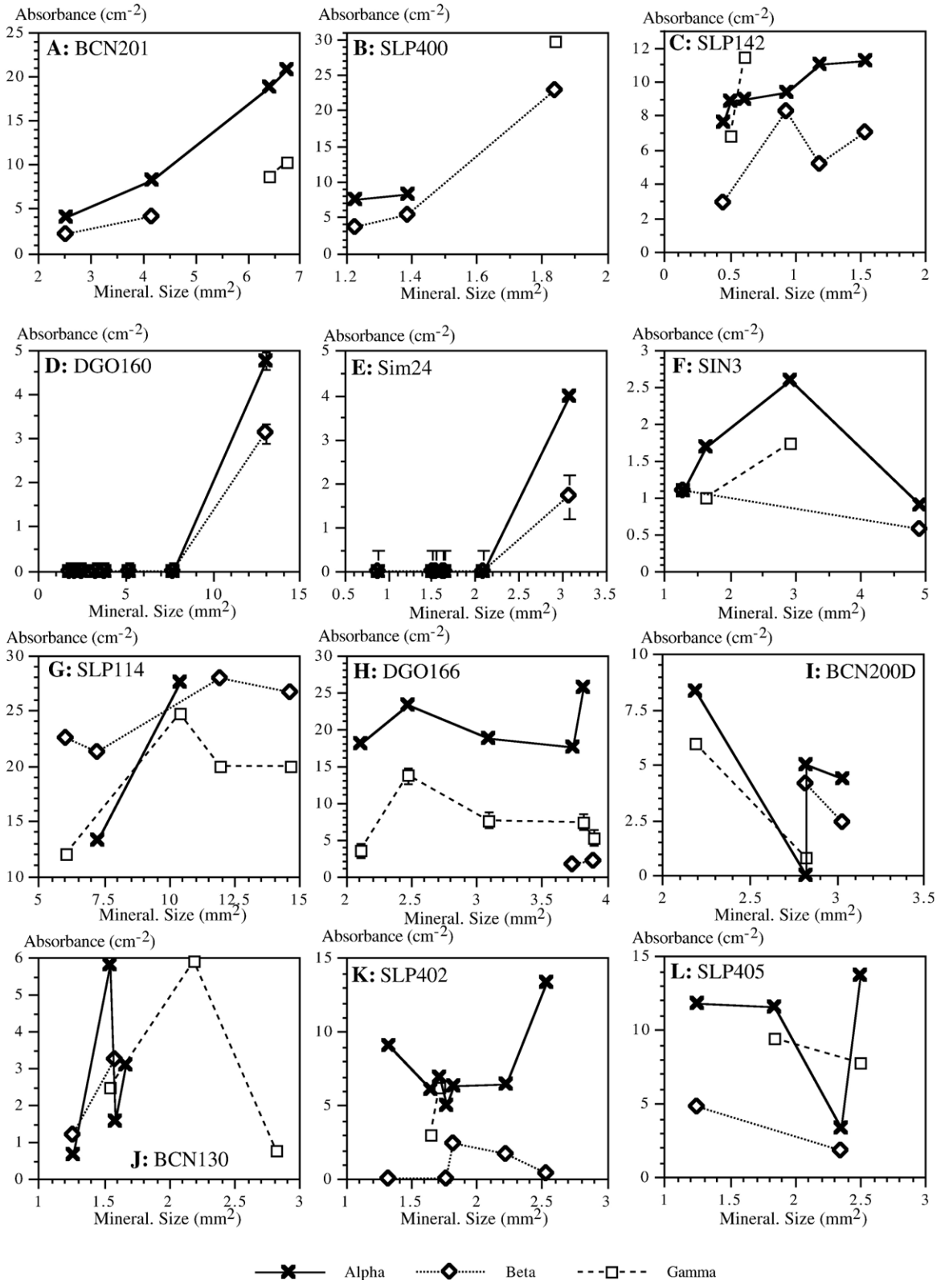
A: BCN201
B: SLP400
C: SLP142
D: DGO160
E: Sim24
F: SIN3
G: SLP114
H: DGO166
I: BCN200D
J: BCN130
K: SLP402
L: SLP405
Absorbance (cm-2)
Mineral. Size (mm2)
Alpha
Beta
Gamma

Table 1
Water contents of olivines expressed as ppm $H_2O$ by weight (Ol $H_2O$ (ppm)), and various parameters mentioned in text

| Location | Sample | Ol $H_2O$ (ppm) | ΔOl $H_2O$ (ppm) | WR $H_2O$ (ppm) | Fo | Cpx La/Yb | Spi $Fe^{3+}/\Sigma$ Fe | ΔFMQ | Fluid inclusions |
|---|---|---|---|---|---|---|---|---|---|
| *Mexico* | | | | | | | | | |
| VE | SLP402 | 4.4 | 0.29 | 109 | 88.3 | 0.70 | 0.19 | 0.0 | avoidable |
| VE | SLP400 | 4.5 | 0.29 | | 81.5 | 2.17 | 0.28 | 0.6 | none |
| VE | SLP403 | 5.4 | 0.36 | 128 | 90.5 | 1.30 | 0.04 | −1.1 | avoidable |
| VE | SLP101 | 1.9 | 0.26 | 49 | 90.4 | | 0.14 | −0.7 | avoidable |
| VE | SLP114 | 6.1 | 0.36 | 30 | 91.3 | 2.68 | 0.21 | 0.1 | avoidable |
| SD | SLP405 | 5.3 | 0.34 | 101 | 89.5 | 0.07 | 0.03 | −1.8 | avoidable |
| SD | SLP142 | 6.0 | 0.39 | 135 | 89.8 | 0.07 | 0.03 | −2.2 | none |
| D | DGO166 | 7.5 | 0.49 | 103 | 89.9 | 0.14 | 0.21 | 0.0 | none |
| D | DGO160 | 1.5 | 0.12 | 28 | 91.6 | 2.56 | 0.26 | 0.5 | none |
| MC | SIN3 | 1.0 | 0.13 | | 89.6 | 0.14 | 0.20 | 0.3 | unavoidable |
| SQ | BCN200D | 3.5 | 0.27 | 154 | 88.8 | 0.33 | 0.11 | −0.2 | none |
| SQ | BCN130 | 2.2 | 0.21 | 77 | 89.3 | 0.66 | 0.26 | 0.2 | rare |
| SQ | BCN201 | 6.6 | 0.43 | 86 | 89.8 | 0.09 | 0.14 | −0.4 | unavoidable |
| SQ | BCN203 | 0.0 | | | 90.6 | 1.88 | 0.13 | 0.0 | avoidable |
| *USA* | | | | | | | | | |
| Simcoe | Sim9c | 0.2 | 0.07 | 25 | 90.7 | 26.07 | 0.27 | 0.3 | rare |
| Simcoe | Sim24 | 1.1 | 0.13 | 41 | 91.0 | 3.73 | 0.39 | 0.9 | avoidable |
| Simcoe | Sim3 | 0.0 | | 27 | 90.7 | 7.77 | 0.38 | 0.8 | avoidable |

Water contents in olivines were calculated using the highest absorption intensities for each sample in each polarizer orientation (see text), so that they are the maximum water content for olivines of each sample. ΔOl $H_2O$ (ppm) is the uncertainty on the water content (see text for details). WR $H_2O$ is the whole-rock water content using olivine values from this table along with previously published pyroxene water contents and mineral modes [30,34,37]. Fo is the forsterite content of olivine expressed as $100\times Mg/(Mg+Fe^{2+})$. Ol=olivine, Cpx=clinopyroxene, Opx=orthopyroxene, Spi=spinel. Fo, Cpx La/Yb, Spi $Fe^{3+}/\Sigma Fe$ and ΔFMQ are from [33,34,37]. The presence of fluid inclusions was checked using a petrographic microscope at 600× magnification.

### 5.1.3. Sample-by-sample assessment

Spectra of SLP114 olivines are unique in that the main absorption intensities are in Group II (Fig. 1). This has never been reported before for a natural olivine from a peridotite, but is expected for its high forsterite content ($Fo_{91.3}$) [18,26]. In SLP400 olivines, the absorption intensity of the large band centered around 3250 $cm^{-1}$ in the $\gamma$ direction has a larger calculated area beneath the peak than any other band in all directions, making the greatest contribution to the total water content. But the heights of the peaks in Group I are larger than those in Group II (Fig. 1), leading us to consider SLP400 in the same category as all other samples except SLP114. Sample SLP400 has low-Fe olivines ($Fo_{81.5}$) and thus has spectra predicted by experiments [26], with the main bands in Group I. Olivines of sample SLP402 also have a relatively low forsterite content ($Fo_{88.3}$) which likely explains the fact that its main absorbance peaks are in Group I. If we assume that olivines with $Fo_{\leq 90}$ should have Group I-dominated spectra, only 5 out of our 15 olivine samples with detectable water have spectra not compatible with experiments: $Fo_{>90}$ olivines from the Simcoe samples and from Mexican samples DGO160, SLP403, and SLP101.

### 5.1.4. Clues to explain Group I dominated spectra in high-Fo olivines

To explain the fact that some high-Fo olivines seem not to have OH FTIR spectra consistent with olivine-orthopyroxene equilibrium, three suggestions have been

Fig. 3. Polarized infrared absorption intensities measured as area beneath the OH peaks at the center of olivine grains versus the size of the olivines, taken as the area of the wafered and polished grains. Only samples for which the orientation was certain are shown. Sim9c is not shown because the uncertainties on the absorbance are too large to make any absorbance vs. grain size relationship significant. Uncertainties are smaller than the symbols except for Sim24 beta (E). For BCN201, DGO160, and Sim24, the larger the olivine, the more water it contains (A, D, E). SLP400, SLP142, and SLP114 (and possibly SIN3) show similar but less consistent patterns (B, C, G, F). This could be due to the way the grain size was measured by calculating the area of the polished grain surface in 2 dimensions only. The 3rd dimension was lost through grinding. A point falling above a correlation in the figure might mean that the grain was thick in that, the 3rd dimension and thus the water concentration at that spot is higher than predicted by the 2 dimensional grain size. The other half of the samples do not show a correlation between water content and grain size. The significance of the correlation between grain size and water content likely means that small olivines have lost their hydrogen faster than the large ones during xenolith ascent to the surface. Samples that clearly lack correlation are DGO166, BCN130, SLP402, and SLP405 (H, J, K, L).

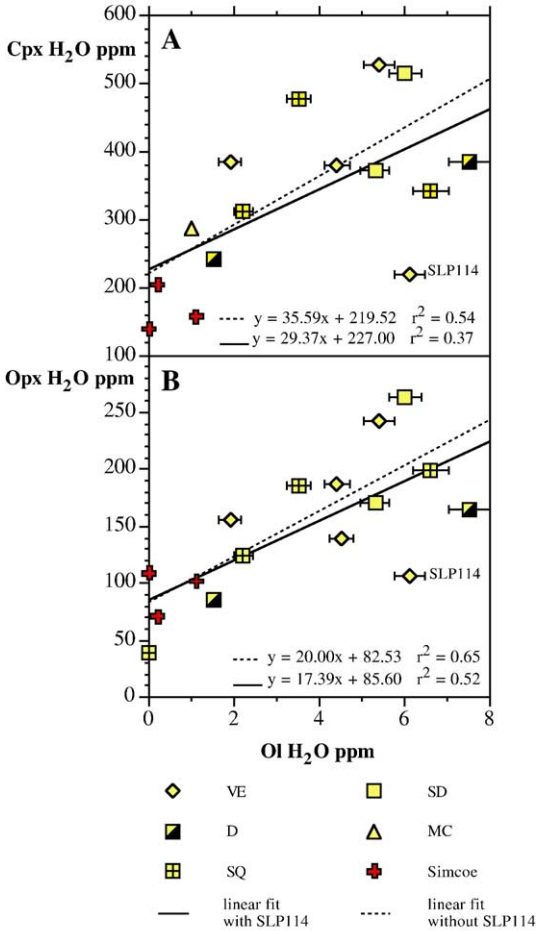


Fig. 4. Water contents in olivine (Ol) versus A: clinopyroxene (Cpx), and B: orthopyroxene (Opx) from Mexican and Simcoe xenoliths. Water contents in olivine increase roughly with those in coexisting pyroxenes, with the best correlation for orthopyroxenes. SLP114 is a Mexican harzburgite that in contrast with all other samples has olivines with the highest OH infrared absorption peaks in Group II (see Fig. 1); SLP114 falls off the correlations for the other samples. Therefore, linear fits are better if SLP114 is excluded. Pyroxene data from Peslier et al. [30]. Error bars for the olivine water contents take into account uncertainties on the background of the spectra and the uncertainty in the absorption coefficient (see text).

made. The spectra might reflect: (1) a former higher pressure state in equilibration with magnesiowüstite [18]; (2) metasomatic overprinting by a low-silica melt or fluid [18]; or (3) hydrogen content of olivine re-equilibrated with that of the host magma [39].

(1) Luhr and Aranda-Gómez [37] described clusters of inter-grown spinel and pyroxene that might be decompression-reaction products of garnet and olivine in only 3 Mexican spinel-peridotite xenoliths: SLP101, SLP403 and DGO160. The latter may thus have come originally from the garnet stability field, but there is no evidence that any of the samples have come from deeper (>410 km) where magnesiowüstite is stable.

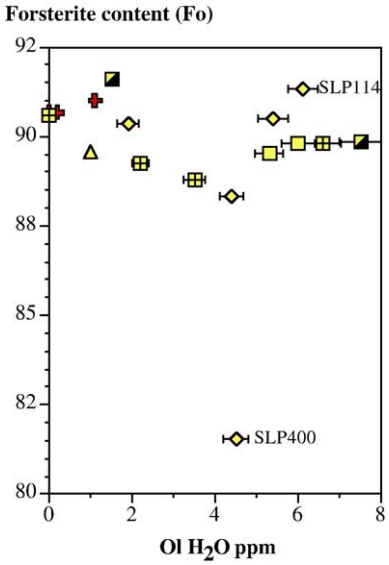


Fig. 5. Water contents versus forsterite contents ($100 \times Mg/Mg+Fe^{2+}$) of olivines from Mexican and Simcoe xenoliths. No correlations are observed between olivine water contents and indices of melt extraction such as forsterite content. Forsterite contents are from Luhr and Aranda-Gómez [37] and Brandon et al. [36]. Symbols as in Fig. 4.

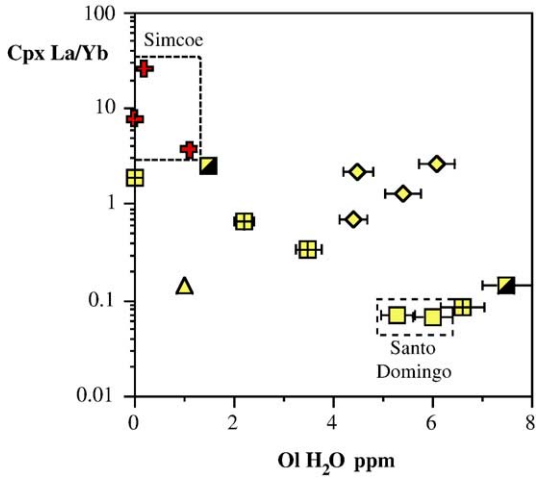


Fig. 6. Olivine water contents versus clinopyroxene La/Yb ratios. Simcoe olivines have among the lowest water contents and the highest La/Yb ratios, symptomatic of the subduction-related metasomatism these xenoliths are interpreted to have undergone [33–36]. Mexican Santo Domingo olivines are relatively water rich and have the lowest clinopyroxene La/Yb ratios. Clinopyroxene La/Yb ratios are taken from Luhr and Aranda-Gómez [37] and Brandon et al. [36]. Symbols as in Fig. 4.

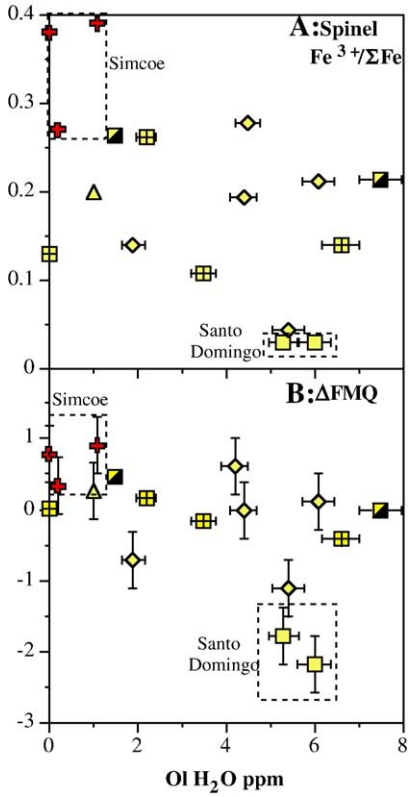


Fig. 7. Olivine water contents versus A: spinel $Fe^{3+}/\Sigma Fe$ and B: resulting calculated oxygen fugacity relative to the fayalite-magnetite-quartz buffer (ΔFMQ). Spinel values are calculated from microprobe data for the Mexican xenoliths [37] and measured by Mössbauer for the Simcoe ones [34]. Simcoe xenoliths are very oxidized, which seems symptomatic of mantle-wedge environments [34], and have little water in their olivines. Symbols as in Fig. 4.

(2) The compositions of Simcoe mantle xenoliths have clearly been influenced by fluids or melts of subduction origin (very high La/Yb ratios in clinopyroxenes for example, Table 1) [33,34,36]. However the presence of phlogopite and/or of alkali- and silica-rich glass in some Simcoe xenoliths points towards a metasomatic agent rich in water but also in silica [36]. Data for the Mexican xenoliths are more limited, but samples DGO160 and SLP403 are among those with the highest clinopyroxene La/Yb ratios (>1; no data for SLP101; [37]). The elevated Mexican La/Yb ratios, however, are due to depleted Yb contents rather than high La contents as found for the Simcoe clinopyroxenes. Consequently metasomatism by low-silica activity melts or fluids in the mantle cannot be proven as the cause of the main olivine OH peaks being in Group I when experiments predict they should be in Group II in Simcoe and in high-Fo Mexican olivines.

(3) Hydrogen loss during xenolith transport to the surface is evident in the analyzed olivines (see below). The original hydrogen accommodated by the silicate framework and acquired in the mantle could have been lost during later emplacement (magma exchange and/or crustal conditions encountered between the mantle and the surface) resulting in disequilibrium of the present hydrogen speciation and the silicate framework [40]. All xenoliths of this study were collected from cinder cones or maars formed by mafic alkalic magmas. The olivine nephelinites that erupted at Ventura-Esperitu-Santo are the most-silica undersaturated volcanic rocks known from the Mexican Basin and Range Province [34,37]. Smaller xenoliths may have undergone more interaction with the host magmas than larger ones. However, DGO 160 (4.5 kg), SLP403 (1.2 kg), SLP101 (0.9 kg), and Simcoe xenoliths (<0.5 kg) span the range of sizes for the samples analyzed [34,37]. Xenolith size thus does not support hydrogen exchange between host-magma and the xenolith and resultant olivine OH spectral modification.

In summary, most olivine OH spectra are in accordance with experimental results. It cannot be proven with certainty if exchange of hydrogen with low-silica activity melts at depth or during transport to the surface is responsible for the difference between observed spectra of some high-Fo olivines and those predicted in experiments.

### *5.2. Water loss from olivines during xenolith transport to Earth's surface*

#### *5.2.1. Hydrogen partition coefficients between olivine and pyroxenes*

The lack of reproducibility of water contents within and among olivine grains for each sample (Figs. 2 and 3) is likely due to hydrogen loss from the olivine during xenolith transport from the mantle to Earth's surface. An estimate was still needed for the olivine water content prior to ascent-related loss to be used for comparison with other compositional parameters in the peridotites. We use water contents (Table 1) calculated from FTIR spectra acquired at the centers of the largest grains for each sample; more precisely the largest values of area beneath the OH peaks in all three directions were used. Because the problem of hydrogen loss was not present in the pyroxenes (reproducibility within and among

grains was good with only a slight decrease of hydrogen content at the very edges of some grains [30]), and because positive correlations exist between water contents of olivines and those of associated pyroxenes (best correlation being with orthopyroxenes, Fig. 4), olivine water contents may still retain useful information from before xenolith transport. Hydrogen partition coefficients determined experimentally [45–48] may be used to calculate how much water was lost during xenolith transport. Our data (Table 1, Fig. 4) generate the following hydrogen partition coefficients between olivine (Ol) and clino- and orthopyroxenes (Cpx and Opx):

$$[H_2O]_{Ol}/[H_2O]_{Cpx} = D_H^{Ol/Cpx} = 1/35.59 = 0.03$$

and

$$[H_2O]_{Ol}/[H_2O]_{Opx} = D_H^{Ol/Opx} = 1/20.00 = 0.05.$$

These values are 10 times lower than partition coefficients calculated from data on natural megacrysts in kimberlites ($D_H^{Ol/Cpx} = 0.33 \pm 0.06$ and $D_H^{Ol/Opx} = 0.63 \pm 0.08$) [40]. Aubaud et al. [46] experimentally determined the following values:

$$D_H^{Ol/Cpx} = 0.08 \pm 0.01$$

and

$$D_H^{Ol/Opx} = 0.11 \pm 0.01.$$

The differences between these natural and experimental partition coefficients emphasize the fact that our olivines lost hydrogen. The amount lost can be calculated from the experimental partition coefficients above. The difference in natural versus experimental values is 37.5% for $D_H^{Ol/Cpx}$ and 45% for $D_H^{Ol/Opx}$. Keeping in mind that this is a minimum estimate because it assumes that pyroxenes did not lose any hydrogen, the centers of xenolith olivine grains thus lost almost half of their hydrogen on their way to the surface.

### *5.2.2. Water-content profiles across olivines and host-magma ascent rates*

Absorption intensities in most analyzed olivine crystals decrease towards the grain edges (Fig. 2) and for about half the samples, smaller grains have less water than larger grains (Fig. 3). This is likely due to protons having diffused out of the olivines while the xenoliths were transported to the surface by the host magmas. Diffusion experiments have shown that hydrogen moves quickly through olivine at 800–1100 °C [3,28]. Hydrogenation experiments result in absorption intensity profiles through olivine grains that are a mirror image of those of Fig. 2 with high water contents at the edges and low water contents in the grain centers [28]. Diffusion profiles like those in Fig. 2 can be modeled by a diffusion equation for a sample of finite size containing homogeneously distributed water, surrounded by an infinite reservoir containing no water, and assuming a coefficient of diffusion independent of hydrogen concentration [49]:

$$C = C_0 \mathrm{erf}(X/2(Dt)^{1/2}) \quad (2)$$

where $C_0$ is the maximum $H_2O$ concentration, $C$ is the $H_2O$ concentration from the grain edge, $X$ is the distance from the grain edge, and $D$ is the diffusion coefficient of hydrogen. This equation, however, models only half of the profile of water content across an olivine grain, i.e. from its center to one of its edges. Another calculation can be made to model the entire profile from rim to rim ($h$) using an infinite series [49] and solving it for the first three terms ($j=0$, $j=1$, and $j=2$).

$$C = 4C_0/\pi \sum_{j=0}^{\infty} 1/(2j+1)\sin\{[(2j+1)\pi X]/h\} \times \exp\{-[(2j+1)\pi/h]^2 Dt\} \quad (3)$$

Fitting these calculated profiles using Eqs. (2) and (3) to our data allows an estimate of how much time it took for the olivine grains to lose their hydrogen (Fig. 2).

An evaluation of the influence of the various parameters in the equations shows that the time of diffusion depends primarily on the diffusion coefficient chosen and the initial concentration of water in the olivine (Fig. 8). Because all experiments to determine diffusion coefficients [50,51] were conducted at about the same temperature, i.e. 1000–1100 °C, temperature is not a variable in the following modeling. An example is shown using an olivine from sample BCN201 in Fig. 8. Both Eqs. (2) and (3) give similar results (Fig. 8). If the calculations are made with the pure diffusion coefficient of hydrogen (maximum range of $6\times10^{-12}$ to $1\times10^{-10}$ $m^2$ $s^{-1}$ [52]), i.e. without taking into consideration the moderating effect of point-defect diffusion, the calculated water concentration decreases 10 fold for a given time across that range ("H only" in Fig. 8C and D). The rate of diffusion for point defects such as metal vacancies is two orders of magnitude slower than that for protons [50]. A more realistic coefficient of diffusion that takes into account the effect of point defects on slowing hydrogen loss ranges from $5\times10^{-13}$ to $5\times10^{-12}$ $m^2$ $s^{-1}$ [50,51], the use of which only results in a small water concentration range for a given time of diffusion ("H+ defects" in Fig. 8C and D). The calculation of diffusion

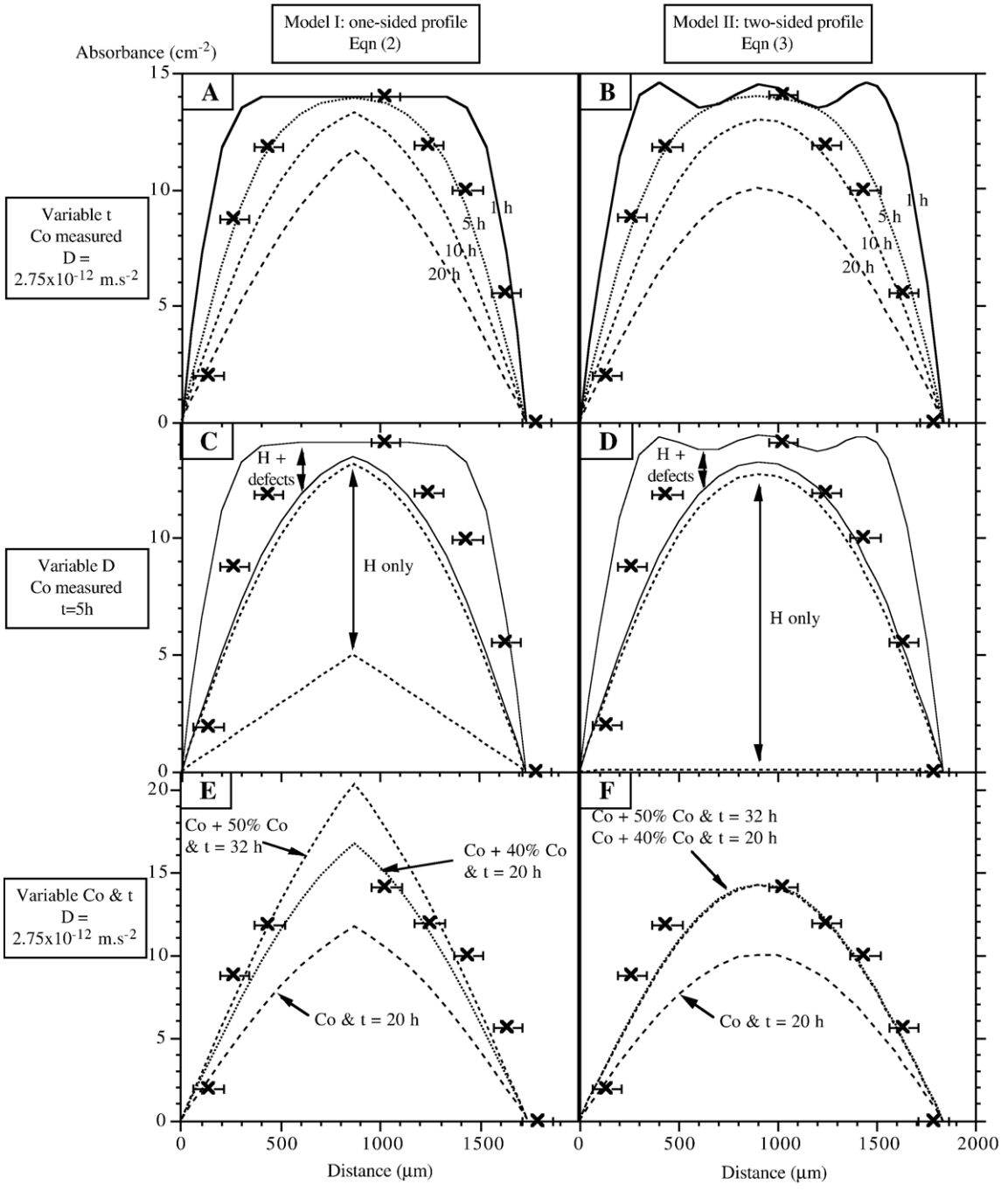


Fig. 8. Calculated hydrogen diffusion profiles using Eqn (2) (Model I) and Eqn (3) (Model II) with varying parameters: $t$, diffusion time; $C_0$, the initial water concentration in the mantle; and $D$, the coefficient of diffusion. Model I provides only a one-sided profile (core to rim) and has been mirrored on the second side to model the entire olivine from rim to rim. The 2 wavy profiles obtained with Model II (B, D) are an artifact resulting from the fact that the infinite series solution was approximated by evaluation of only the first 3 terms ($j=0$ to $j=2$). These calculated diffusion profiles are superimposed on the water content cross section of Olivine 15 of sample BCN201 in the alpha direction (black crosses). A and B: $t$ is the only variable, $C_0=14.04$ cm$^{-2}$ and $D=2.75\times10^{-12}$ m s$^{-1}$. C and D: $D$ is the only variable and the curves are for the extreme values determined experimentally [50,51], $C_0=14.04$ cm$^{-2}$ and $t=5$ h. E and F: $C_0$ and $t$ vary, $D=2.75\times10^{-12}$ m s$^{-1}$. $C_0$ measured = water concentration measured at the center of BCN201 olivine 15 in the alpha direction (14.04 cm$^{-2}$). "H only" shows the field spanning the coefficients of diffusion for proton diffusion only [50]. "H + defects" shows the field spanning the coefficients of diffusion for a combination of proton and point-defect diffusion through the olivine [50,51]. See text for details.

time for all other samples (Fig. 2) was done with the mean of these 2 extreme diffusion coefficients that take the point defect diffusion into account ($5\times10^{-13}$ and $5\times10^{-12}$ $m^2$ $s^{-1}$), i.e. a value of $2.75\times10^{-12}$ $m^2$ $s^{-1}$. The water concentration in the center of the olivine decreases with time (Fig. 2A and B). Modeling a profile can be achieved in 2 ways: either with a low initial water concentration and a short diffusion time (for example in Fig. 8A and B: $C_0$ measured by FTIR at the center of the olivine and $t$=5 h) or with a higher initial water concentration combined with a longer diffusion time (for example in Fig. 8E and F: 40–50% more water than measured by FTIR at the center of the olivine and $t$=20–30 h).

Because the water concentration measured at the center of the largest olivine grains (Table 1, Fig. 4) is probably 40% lower than the initial water concentration in the mantle, the profiles of Fig. 2 were modeled using the second method. When water profiles could be measured on 2 olivines of different sizes from the same sample (Fig. 2A and B), the $C_0$ of the smaller olivine has to be adjusted to that of the larger one so that the times of hydrogen loss are consistent. For example modeling profiles across relatively small grain Olivine 10 from BCN201 gives a time of 8 h, but 20 h is obtained for the relatively large grain Olivine 15, both using the $C_0$ measured at the centers of the respective grains plus 40%. But, using the $C_0$ of Olivine 15 (+40%) to model the profile across Olivine 10 requires a time of 18 h, i.e. consistent with the time calculated from Olivine 15 profiles (Fig. 2A and B). A similar result is obtained for sample SLP114 with larger Olivine 19 and smaller Olivine 16 (Fig. 2C and D).

The resulting calculated times of hydrogen loss thus vary from 18 to 65 h (Fig. 2). Using the equilibration pressures calculated for the samples and resulting depth of mantle origin (34.5 km for BCN201 and 40.4 km for SLP114) [37], these times of hydrogen loss correspond to host magma ascent rates of 0.2–0.5 m $s^{-1}$. These calculated magma ascent velocities can be compared to those estimated for similar xenolith-bearing host magmas based on laboratory studies of olivine and pyroxene xenocryst dissolution rates (surface reached in less than a day, which for a source depth of 40 km translates to >0.5 m $s^{-1}$) [53,54] or on calculations of xenolith settling velocities in the host magmas (0.01–5 m $s^{-1}$) [55]. In the experiments, important parameters such as shocks and tumbling are difficult to reproduce, and other factors such as stress and strain of the surrounding mantle and crustal rocks the magma passes through are not taken into account. However, the hydrogen loss estimates in this study are in the range of these earlier estimates.

### 5.3. Water contents in the sub-continental lithospheric mantle

#### 5.3.1. Parameters controlling hydrogen incorporation by olivine

As much as half of the hydrogen in the studied olivines may have diffused out during transport to the surface. However, because the amounts of water in olivines and coexisting pyroxenes are correlated, and because the pyroxenes do not show the signs of hydrogen loss so evident for the olivines, it is logical that any relationship between original water content and partial melting or any other mantle process that influences hydrogen incorporation by olivine would have been retained.

Hydrogen behaves as an incompatible element during partial melting [46] and thus less of it would be expected in the high-Fo olivines compared to the low-Fo ones. The lack of such a correlation with indices of melting such as forsterite content (Fig. 5) indicates either that the relationship existed at depth but was erased during later hydrogen loss, or that partial melting is not the main control on hydrogen incorporation in olivines in the mantle.

Metasomatism by melts or fluids may also be responsible for the variation of olivine water contents. There is no correlation, however, between water in olivines and the La/Yb ratio of coexisting clinopyroxenes (Fig. 6) which is generally higher in metasomatized peridotites (such as Simcoe xenoliths) compared to those that only underwent partial melting [31]. Only Simcoe olivines have very high clinopyroxene La/Yb ratios and low water contents compared to the other samples. But as shown above, their OH spectra do not seem to correspond to the type of metasomatic melt that is the most likely for these rocks. The two samples with the lowest clinopyroxene La/Yb ratios (from Santo Domingo) have among the highest olivine water contents (Fig. 6). Interestingly Santo Domingo nodules include, besides the peridotites analyzed in this study, kaersutite megacrysts and kaersutite-bearing xenoliths of mantle origin, suggesting that the mantle sampled at this location is rich in water-bearing fluids or melts.

In the light of negative correlations between water content of pyroxenes and calculated oxygen fugacity, Peslier et al. [30] suggested that the main control on hydrogen incorporation by these minerals may be the oxygen fugacity of the ambient mantle peridotite. There is not as clear a correlation as with the pyroxenes between olivine water concentrations and spinel $Fe^{3+}/\Sigma Fe$ ratios or resulting calculated oxygen

fugacities expressed as ΔFMQ (Fig. 7). But Simcoe samples define one end of the trend with high oxygen fugacities and low water contents, and Santo Domingo samples define the other end at low oxygen fugacities and high water contents. The mechanism of hydrogenation/dehydrogenation of mantle minerals is believed to be mainly dependant of the reduction–oxidation of iron [56–58]

$$Fe^{3+} + O^{2-} + 1/2H_2 = Fe^{2+} + OH^-. \quad (4)$$

This equilibrium implies that hydrogen loss from mantle minerals should be accompanied by $Fe^{3+}$ content increase in that mineral, and conversely hydrogen gain would result in a decrease in $Fe^{3+}$. This is consistent with our data on pyroxenes and possibly olivine if we assume that the $Fe^{3+}$ content of these minerals (not analyzed) and that of spinel are positively correlated. But what caused the inverse variation of mantle-mineral water and spinel $Fe^{3+}$ contents (admittedly poor for olivines); is it hydrogen loss during magma transport or hydrogen acquisition in the mantle prior to ascent? Theoretically, $Fe^{3+}$ in pyroxenes and olivines should increase during ascent if Eq. (4) is the main mechanism of hydrogen loss [56]. Peslier et al. [30] suggested that hydrogen loss could be ruled out for the pyroxenes because their water contents correlated with various chemical parameters not disturbed by xenolith transport. In particular water content was negatively correlated with $Fe^{3+}/\Sigma Fe$ of spinel, a mineral where no hydrogen has ever been detected [1], and thus whose $Fe^{3+}$ content will not be modified by host-magma ascent through the mechanism of Eqn (4). Interestingly, olivines cannot accommodate much $Fe^{3+}$ [59–61]. $Fe^{3+}$, however, has been detected by Mössbauer in an olivine containing 1200 ppm $H_2O$ at 12 GPa, but not in a dry one at 4 GPa [62]. Moreover, for a given hydrogen fugacity, hydrogen solubility in olivine increases with increasing oxygen fugacity [15]. These two results suggest that the more hydrogen in olivine, the more $Fe^{3+}$, i.e. the opposite of what Eq. (4) implies. These experimental results [15,62] were from olivines at solubility levels for hydrogen and thus may not be representative of the situation in the mantle where the availability of water may be limited. Oxidation of the environment may still be the main controlling parameter for the incorporation of hydrogen in upper-mantle minerals, but the signal for this phenomenon may be partially erased in olivines as they lose water during transport to the surface.

*5.3.2. Olivine water contents in various mantle settings*

The Mexican xenoliths represent typical off-craton sub-continental mantle beneath Proterozoic terrains. When compared to olivine water concentrations from cratonic mantle xenoliths (10–70 ppm) [1,20,29], the water content of olivine from Mexican peridotites (<10 ppm) are considerably lower (Fig. 9). Two hypotheses could explain the difference: (1) fundamentally different water contents in these two mantle domains or (2) different host-magma ascent rates.

(1) The main difference between xenoliths from cratons versus those from off-craton is that the former come from deeper (mainly garnet stability field) [63] and from a more reduced environment [64]. Higher pressure increases the solubility of hydrogen in olivine [24] but more reducing conditions decreases it [15], thus having opposing influences. However, again, saturation may not have been reached in these mantle settings, and the water content difference between the two mantle environments may just reflect that the cratonic mantle is wetter than the mantle beneath mobile belts. Although the cratonic mantle is very depleted (high proportion of harzburgites and high-Mg lherzolites), many observations point towards their flushing by wet melts [65,66]. The higher water contents in olivines from cratonic mantle could then indicate that the mantle was more hydrous during the Archean than it is at present.

(2) The mantle xenoliths studied here were brought up by various mafic alkalic magmas with magma-ascent rates estimated in the range 0.2–0.5 m $s^{-1}$. Mantle xenoliths from cratons typically are brought up by kimberlite magmas, whose ascent rates are thought to be about 4 m $s^{-1}$ [67] or 10–30 m $s^{-1}$ [54], i.e. higher than that of mafic alkalic magmas calculated in this study. Moreover, pyroxene water contents are similar in both cratonic (Cpx: 370–500 ppm, Opx: 180–460 ppm) [2] and off-cratonic settings (Cpx: 150–530 ppm, Opx: 40–260 ppm) [2,30]. As mentioned above, pyroxenes seem mostly immune to water loss during xenolith transport in contrast to olivine [30]. As only olivine shows differences in water content between the two mantle settings, the difference in host-magma ascent rates is likely the cause for the higher water contents measured in olivines from cratonic mantle xenoliths compared to those from off-craton xenoliths.

More recent subduction zones are worth examining because minerals from the mantle wedge could have

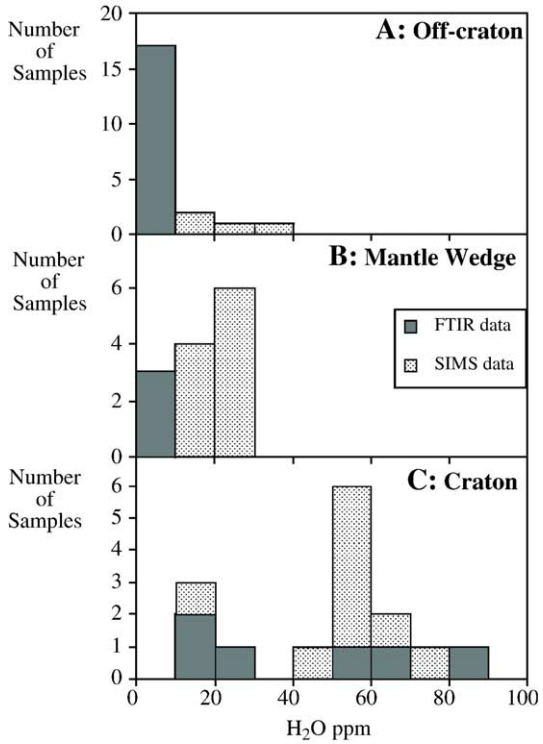


Fig. 9. Histograms of water contents in olivines from mantle xenoliths in 3 different domains of continental lithospheric mantle: A: off-craton (Mexico, this paper; Kilbourne Hole, NM, USA; West Kettle River, BC, Canada [2]; San Carlos, AZ, USA; Eifel, Germany [29]), B: mantle wedge (Simcoe, this paper; various Japanese locations [29]), and C: craton (various locations in South Africa and Lesotho [2,29]). FTIR (this paper and [2]) and SIMS [29] analyses are shown in different shades of grey to emphasize that SIMS data may overestimate water contents in olivines as seems to be especially the case for the off-craton and mantle-wedge settings. Overall, olivines from the mantle beneath cratons have more water than olivines from the mantle beneath continental mobile belts.

different water contents than those from other continental mantle settings. Based on low pyroxene water contents, Peslier et al. [30] argued that the mantle-wedge minerals do not retain any water coming from the slab, possibly because of the oxidizing nature the subduction fluids or melts (see Eq. (4)). The olivines from the same samples, the subduction-metasomatized Simcoe xenoliths, also have lower water concentrations compared to those of the Mexican samples (Fig. 4), thus apparently confirming this interpretation. However, analyses of mantle-xenolith olivines from Japanese subduction zones [29] seem to indicate that the Simcoe olivines have exceptionally low water contents (Fig. 9). More olivine data are thus needed on subduction zones to determine if mantle wedges have "wet" anhydrous mantle minerals or "dry" ones.

### 5.3.3. Water content of the Earth's mantle

Having measured water in pyroxenes [30] and olivines (this paper) from the same samples, a calculation of the whole-rock water content can be achieved using the mineral modes. Hydrogen has never been detected in spinels [1] so they do not enter the calculation. The whole-rock water contents in the Mexican and Simcoe peridotites range from 25 to 154 ppm $H_2O$ (Table 1). These values are minima because olivines have probably lost at least 40% of their hydrogen. However, because olivines have so much less water than the pyroxenes, the whole-rock water contents hardly change if the olivine values are increased by 40%. The whole-rock water contents listed in Table 1 thus constitute the best estimate so far for the amount of water in the lithospheric mantle at the pressures of the spinel stability field. The storage capability of water in mantle minerals changes with pressure, being estimated to be 4000 ppm just above the mantle transition zone (410–660 km), and to increase with depth to a maximum of 6000 ppm around 350 km depth [27]. These numbers of course represent a theoretical upper solubility limit characterized by mantle minerals so full of hydrogen that any more would have to go in another phase (fluid or melt). Nevertheless, if 150 ppm is speculated to be representative of the water content of the entire upper

mantle (to 410 km), it translates into 0.06 times the oceans' mass, i.e. much less water than is thought to be retained in the mantle transition zone (2 to 4 times the mass of the oceans) [68,69].

## 6. Conclusion

Olivines from spinel-peridotite mantle xenoliths lost as much as half of their hydrogen during transport to the surface. Care must be taken in interpreting water contents of olivines from xenoliths as representative of their mantle-source regions. Analysis of hydrogen in olivines from mantle xenoliths should be done on spots in the middle of the largest grains for each sample. Crystal zoning profiles and variations with grain size should also be evaluated to document possible hydrogen loss during ascent. Variations of water contents within olivines allows the calculation of host-magma ascent rates of up to 0.5 m $s^{-1}$, in agreement with previous estimates for ascent rates of peridotite-bearing mafic alkalic magmas. Olivines from xenoliths in kimberlite magmas erupted in cratonic settings appear to have more water than those from xenoliths in mafic alkalic volcanic rocks from off-craton sub-continental lithosphere, such as analyzed here. The difference may be due to higher magma ascent rates of kimberlites compared to those of mafic-alkalic magmas. Despite the dramatic loss of hydrogen from the olivines, their water contents are so low compared to those of pyroxenes that the whole-rock water content is hardly modified if the values measured here are taken at face value or if they were 10 times higher. If a whole-rock water content of 150 ppm, the upper value of the range obtained here, is taken as representative of the entire upper mantle, it constitutes a mass of water 2 orders of magnitude less than that of the Earth's oceans.

## Acknowledgments

A.H.P. is very grateful to Lindsay Keller and Richard Morris for letting her use the FTIR at NASA-Johnson Space Center for this study. Occasional help by Keiko Nakamura and George-Ann Robinson was also much appreciated. The authors would like to thank the following people for very helpful and insightful discussions: David Bell, Alan D. Brandon, Cin-Ty A. Lee, Elizabeth Johnson, James K. Meen, Jed Mosenfelder, and George Rossman. Reviews by D. Bell and an anonymous reviewer greatly improved this manuscript. We thank Alan D. Brandon for giving us the Simcoe samples. Finally thank you to the Lunar and Planetary Science Institute in Houston and Steve Mackwell who made possible AHP's access to NASA-JSC grounds.

## Appendix A. Supplementary material

Supplementary data associated with this article can be found, in the online version, at doi:10.1016/j.epsl.2005.12.019.

## References

[1] D.R. Bell, G.R. Rossman, Water in Earth's mantle: the role of nominally anhydrous minerals, Science 255 (1992) 1391–1397.
[2] D.R. Bell, Water in mantle minerals, Nature 357 (1992) 646–647.
[3] S.J. Mackwell, D.L. Kohlstedt, M.S. Paterson, The role of water in the deformation of olivine single crystals, J. Geophys. Res. 90 (1985) 11319–11333.
[4] S. Mei, D.L. Kohlstedt, Influence of water on plastic deformation of olivine aggregates: 2. Dislocation creep regime, J. Geophys. Res. 105 (2000) 21471–21481.
[5] S. Mei, D.L. Kohlstedt, Influence of water on plastic deformation of olivine aggregates: 1. Diffusion creep regime, J. Geophys. Res. 105 (2000) 21457–21469.
[6] G. Hirth, D.L. Kohlstedt, Rheology of the upper mantle and the mantle wedge: a view from the experimentalists, in: J. Eiler (Ed.), Inside The Subduction Factory, Geophysical Monograph Series, vol. 118, Am. Geophys. Union, 2004, pp. 83–106.
[7] A.M. Hofmeister, Enhancement of radiative transfer in the upper mantle by OH-in minerals, Phys. Earth Planet. Inter. 146 (2004) 483–495.
[8] S. Karato, H. Jung, Water, partial melting and the origin of the seismic low velocity and high attenuation zone in the upper mantle, Earth Planet. Sci. Lett. 157 (1998) 193–207.
[9] S. Karato, The role of hydrogen in the electrical conductivity of the upper mantle, Nature 347 (1990) 272–273.
[10] S. Hier-Majumder, I.M. Anderson, D.L. Kohlstedt, Influence of protons on Fe–Mg interdiffusion in olivine, J. Geophys. Res. 110 (2005) B02202.
[11] D.H. Green, Experimental melting studies on a model upper mantle composition at high pressure under $H_2O$-saturated and $H_2O$ undersaturated conditions, Earth Planet. Sci. Lett. 19 (1973) 37–45.
[12] K. Hirose, T. Kawamoto, Hydrous partial melting of lherzolite at 1 GPa: the effect of $H_2O$ on the genesis of basaltic magmas, Earth Planet. Sci. Lett. 133 (1995) 463–473.
[13] A. Beran, A. Putnis, A model of the OH position in olivine, derived from infrared-spectroscopic investigations, Phys. Chem. Miner. 9 (1983) 57–60.
[14] G.H. Miller, G.R. Rossman, G.E. Harlow, The natural occurrence of hydroxide in olivine, Phys. Chem. Miner. 14 (1987) 461–472.
[15] Q. Bai, D.L. Kohlstedt, Effects of chemical environment on the solubility and incorporation mechanism for hydrogen in olivine, Phys. Chem. Miner. 19 (1993) 460–471.
[16] D. Sykes, G.R. Rossman, D.R. Veblen, E.S. Grew, Enhanced H and F incorporation in borian olivine, Am. Mineral. 79 (1994) 904–908.
[17] E. Libowitzky, A. Beran, OH defects in forsterite, Phys. Chem. Miner. 22 (1995) 387–392.

[18] S. Matveev, H.S.C. O'Neill, C. Ballhaus, W.R. Taylor, D.H. Green, Effect of silica acticity on OH-IR spectra of olivine: implications for low-a$SiO_2$ mantle metasomatism, J. Petrol. 42 (2001) 721–729.
[19] N.R. Khisina, R. Wirth, M. Andrut, A.V. Ukhanov, Extrinsic and intrinsic mode of hydrogen occurrence in natural olivines: FTIR and TEM investigation, Phys. Chem. Miner. 28 (2001) 291–301.
[20] A.J.R. Kent, G.R. Rossman, Hydrogen, lithium, and boron in mantle-derived olivine: the role of coupled substitutions, Am. Mineral. 87 (2002) 1432–1436.
[21] S. Matveev, M. Portnyagin, C. Ballhaus, R. Brooker, C.A. Geiger, FTIR spectrum of phenocryst olivine as a indicator of silica saturation in magmas, J. Petrol. 46 (2005) 603–614.
[22] Q. Bai, D.L. Kohlstedt, Substantial hydrogen solubility in olivine and implications for water storage in the mantle, Nature 357 (1992) 672–674.
[23] S.C. Kohn, Solubility of $H_2O$ in nominally anhydrous mantle minerals using $^1H$ MAS NMR, Am. Mineral. 81 (1996) 1523–1526.
[24] D.L. Kohlstedt, H. Keppler, D.C. Rubie, Solubility of water in the a, b and g phases of $(Mg,Fe)_2SiO_4$, Contrib. Mineral. Petrol. 123 (1996) 345–357.
[25] D.R. Bell, G.R. Rossman, J. Maldener, D. Endisch, F. Rauch, Hydroxide in olivine: a quantitative determination of the absolute amount and calibration of the IR spectrum, J. Geophys. Res. 108 (2003), doi:10.1029/2001JB000679.
[26] Y.-H. Zhao, S.B. Gincberg, D.L. Kohlstedt, Solubility of hydrogen in olivine: dependance on temperature and iron content, Contrib. Mineral. Petrol. 147 (2004) 155–161.
[27] M.M. Hirschmann, C. Aubaud, A.C. Withers, Storage capacity of $H_2O$ in nominally anhydrous minerals in the upper mantle, Earth Planet. Sci. Lett. 236 (2005) 167–181.
[28] S.J. Mackwell, D.L. Kohlstedt, Diffusion of hydrogen in olivine: implications for water in the mantle, J. Geophys. Res. 95 (1990) 5079–5088.
[29] M. Kurosawa, H. Yurimoto, S. Sueno, Patterns in the hydrogen and trace element compositions of mantle olivines, Phys. Chem. Miner. 24 (1997) 385–395.
[30] A.H. Peslier, J.F. Luhr, J. Post, Low water contents in pyroxenes from spinel-peridotites of the oxidized, sub-arc mantle wedge, Earth Planet. Sci. Lett. 201 (2002) 69–86.
[31] F.A. Frey, M. Prinz, Ultramafic inclusions from San Carlos, Arizona: petrologic and geochemical data bearing on their petrogenesis, Earth Planet. Sci. Lett. 38 (1978) 129–176.
[32] R.P. Riddihough, Recent movements of the Juan de Fuca plate system, J. Geophys. Res. 89 (1984) 6980–6994.
[33] A.D. Brandon, R.A. Creaser, S.B. Shirey, R.W. Carlson, Osmium recycling in subduction zones, Science 272 (1996) 861–864.
[34] A.D. Brandon, D.S. Draper, Constraints on the origin of the oxidation state of mantle overlying subduction zones: an example from Simcoe, Washington, USA, Geochim. Cosmochim. Acta 60 (1996) 1739–1749.
[35] A.D. Brandon, D.S. Draper, Reply to the comment by B.R. Frost and C. Ballhaus on "Constraints on the origin of the oxidation state of mantle overlying subduction zones: an example from Simcoe, Washington, USA", Geochim. Cosmochim. Acta 62 (1998) 333–335.
[36] A.D. Brandon, H. Becker, R.W. Carlson, S.B. Shirey, Isotopic constraints on time scales and mechanisms of slab material transport in the mantle wedge: evidence from the Simcoe mantle xenoliths, Washington, USA, Chem. Geol. 160 (1999) 387–407.
[37] J.F. Luhr, J.J. Aranda-Gómez, Mexican peridotite xenoliths and tectonic terranes: correlations among vent, location, texture, temperature, pressure, and oxygen fugacity, J. Petrol. 38 (1997) 1075–1112.
[38] E. Libowitzky, G.R. Rossman, Principles of quantitative absorbance measurements in anisotropic crystals, Phys. Chem. Miner. 23 (1996) 319–327.
[39] C. Lemaire, S.C. Kohn, R.A. Brooker, The effect of silica activity on the incorporation mechanisms of water in synthetic forsterite: a polarized infrared spectroscopic study, Contrib. Mineral. Petrol. 147 (2004) 48–57.
[40] D.R. Bell, G.R. Rossman, R.O. Moore, Abundance and partitioning of OH in a high pressure magmatic system: megacrysts from the Monestary kimberlite, South Africa, J. Petrol. 45 (2004) 1539–1564.
[41] G.R. Rossman, Studies of OH in nominally anhydrous minerals, Phys. Chem. Miner. 23 (1996) 299–304.
[42] E. Roedder, Fluid Inclusions, Mineralogical Society of America, 1984, 644 pp.
[43] K. Wright, C.R.A. Catlow, A computer simulation study of (OH) defects in olivine, Phys. Chem. Miner. 20 (1994) 515–518.
[44] D.S. Draper, Spinel lherzolite xenoliths from Loreta Butte, Simcoe Mountains, southern Washington (USA), J. Geol. 100 (1992) 766–776.
[45] K.T. Koga, E. Hauri, M.M. Hirschmann, D. Bell, Hydrogen concentration analyses using SIMS and FTIR: comparison and calibration for nominally anhydrous minerals, Geochem. Geophys. Geosyst. 4 (2003) 1019, doi:10.1029/2002GC000378.
[46] C. Aubaud, E. Hauri, M.M. Hirschmann, Hydrogen partition coefficients between nominally anhydrous minerals and basaltic melts, Geophys. Res. Lett. 31 (2004), doi:10.1029/2004GL021341.
[47] E.H. Hauri, G.A. Gaetani, T.H. Green, Partioning of $H_2O$ between mantle minerals and silicate melts, in: G.e.C. Acta (Ed.), Goldschmidt, vol. 68, Elsevier, Copenhagen, 2004, p. A33.
[48] K. Grant, S.C. Kohn, R. Brooker, Hydrogen partitioning between synthetic olivine, orthopyroxene and melt, in: G.e.C. Acta (Ed.), Goldschmidt, vol. 68, Elsevier, Copenhagen, 2004, p. A33.
[49] P.G. Shewmon, Diffusion In Solids, J. Williams Book Company, Jenks, OK, 1983.
[50] D.L. Kohlstedt, S.J. Mackwell, Diffusion of hydrogen and intrinsic point defects in olivine, Ztg. Phys. Chem. 207 (1998) 147–162.
[51] S. Demouchy, S. Mackwell, Water diffusion in synthetic iron-free forsterite, Phys. Chem. Miner. 30 (2003) 486–494.
[52] D.L. Kohlstedt, S.J. Mackwell, Solubility and diffusion of "water" in silicate minerals, in: K. Wright, R. Catlow (Eds.), Microscopic Properties and Processes in Minerals, Kluwer Academic, Netherlands, 1999, pp. 539–559.
[53] B.R. Edwards, J.K. Russel, A review and analysis of silicate mineral dissolution experiments in natural silicate melts, Chem. Geol. 130 (1996) 233–245.
[54] M. Brearley, C. Scarfe, Dissolution rates of upper mantle minerals in an alkali basalt melt at high pressure: an experimental study and implications for ultramafic xenolith survival, J. Petrol. 27 (1986) 1157–1182.
[55] F.J. Spera, Dynamics of translithospheric migration of metasomatic fluids and alkaline magma, in: M.A. Menzies, C.J. Hawkesworth (Eds.), Mantle Metasomatism, Academic Press, London, 1987, pp. 1–20.

[56] J. Ingrin, H. Skogby, Hydrogen in nominally anhydrous upper-mantle minerals: concentration levels and implications, Eur. J. Mineral. 12 (2000) 543–570.
[57] R. Stalder, H. Skogby, Hydrogen diffusion in natural and synthetic orthopyroxene, Phys. Chem. Miner. 30 (2003) 12–19.
[58] G.D. Bromiley, H. Keppler, C.A. McCammon, F.A. Bromiley, S. D. Jacobsen, Hydrogen solubility and speciation in natural, gem-quality chromian diopside, Am. Mineral. 89 (2004) 941–949.
[59] D. Canil, H.S.C. O'Neill, D.G. Pearson, R.L. Rudnick, W.F. McDonough, D.A. Carswell, Ferric iron in peridotites and mantle oxidation states, Earth Planet. Sci. Lett. 123 (1994) 205–220.
[60] M.D. Dyar, A.V. McGuire, R.D. Ziegler, Redox equilibria and crystal chemistry of coexisting minerals from spinel lherzolite mantle xenoliths, Am. Mineral. 74 (1989) 969–980.
[61] N.C. Richmond, J.P. Brodholt, Incorporation of $Fe^{3+}$ into forsterite and wadsleyite, Am. Mineral. 85 (2000) 1155–1158.
[62] C.A. McCammon, D.J. Frost, J.R. Smyth, H.M.S. Laustsen, T. Kawamoto, N.L. Ross, P.A. van Aken, Oxidation state of iron in hydrous mantle phases: implications for subduction and mantle oxygen fugacity, Phys. Earth Planet. Inter. 143–144 (2004) 157–169.
[63] C.J. Hawkesworth, M.J. Norry (Eds.), Continental Basalts and Mantle Xenoliths, Shiva, Cheshire, 1983, 272 pp.
[64] A.B. Woodland, M. Koch, Variation in oxygen fugacity with depth in the upper mantle beneath the Kaapvaal craton, Southern Africa, Earth Planet. Sci. Lett. 214 (2003) 295–310.
[65] P.B. Kelemen, S.R. Hart, S. Bernstein, Silica enrichment in the continental upper mantle via melt/rock reaction, Earth Planet. Sci. Lett. 164 (1998) 387–406.
[66] A.H. Wilson, S.B. Shirey, R.W. Carlson, Archean ultra-depleted komatiites formed by hydrous melting of cratonic mantle, Nature 423 (2003) 858–861.
[67] S.P. Kelley, J.-A. Wartho, Rapid kimberlite ascent and significance of Ar–Ar ages in xenolith phlogopites, Science 289 (2000) 609–611.
[68] J.R. Smyth, A crystallographic model for hydrous wadsleyite (b-$Mg_2SiO4$): an ocean in the Earth's interior? Am. Mineral. 79 (1994) 1021–1024.
[69] J.R. Smyth, D.J. Frost, The effect of water on the 410-km discontinuity: an experimental study, Geophys. Res. Lett. (2002) 1–5 (2002GL014418).